Distance-dependent emission spectrum from two qubits in a strong-coupling regime

Rongzhen Hu, JunYan Luo, and Yiying Yan [*]

Department of Physics, School of Science, Zhejiang University of Science and Technology, Hangzhou 310023, China

We study the emission spectrum of two distant qubits strongly coupled to a waveguide by using the numerical and analytical approaches, which are beyond the Markovian approximation and the rotating-wave approximation. The numerical approach combines the Dirac-Frenkel time-dependent variational principle with the multiple Davydov D_1 ansatz. A transformed rotating-wave approximation (TRWA) treatment and a standard perturbation (SP) are used to analytically calculate the emission spectrum. It is found that the variational approach and the TRWA treatment yield accurate emission spectra of the two distant qubits in certain strong-coupling regimes while the SP breaks down. The emission spectrum is found to be asymmetric irrespective of the two-qubit distance and exhibits a single peak, double peaks, and multiple peaks depending on the two-qubit distance as well as the initial states. In sharp contrast with the single-qubit case, the excited-state populations of the two qubits can ultraslowly decay due to the subradiance even in the presence of a strong qubit-waveguide coupling, which in turn yields an ultranarrow emission line. Our results provide insights into the emission spectral features of the two distant qubits in the strong light-matter coupling regime.

I. INTRODUCTION

Few distant emitters interacting with electromagnetic fields have received much attention, which is fundamentally relevant to the building block of quantum networks [1,2] and gates [3,4] and also provide a test bed to study a variety of phenomena such as quantum interference [5,6], collective emission such as superradiance and subradiance [7–20], photon-mediated interaction [21,21–25], and quantum entanglement [26–32]. Particularly, the literature has illustrated that the non-Markovianity of the two distant emitters arises from delay-feedback effects due to the field propagating between the distant emitters [33], which strongly influences the collective dynamics of the emitters as well as the spontaneous emission.

Recently, the two-atom problem has been renewed in terms of artificial atoms coupled to a waveguide, which allows the access to the coupling regimes from weak to ultrastrong light-matter interaction [34,35]. For instance, Ref. [36] reports the observation of a large collective Lamb shift of two distant superconducting artificial atoms. With the rotating-wave approximation (RWA), the investigation has revealed the delay-induced non-Markovian features of the spontaneous emission spectrum of two distant qubits weakly coupled to a one-dimensional waveguide, that is, the linewidth broadening beyond standard superradiance and narrow Fano-resonance-like peaks [37]. In the ultrastrong-coupling regime, the photon-mediated interaction between the two distant qubits and the qubit frequency renormalization are found to be significant and play a crucial role in the collective dynamics of the two-qubit system [38]. However, the spontaneous emission spectrum from two distant emitters has not yet been explored in the strong light-matter coupling regime. This acquires a non-Markovian and non-RWA approach that properly takes into account strong-coupling effects.

One way to theoretically calculate the emission spectrum of two distant qubits is the time-dependent variational approach equipped with the multiple Davydov ansatz [39]. This approach has been applied to a variety of models ranging from the quantum Rabi model [40] to the Holstein model [41,42] and has been benchmarked with other numerical methods such as the time-dependent numerical renormalization group [43,44], the quasiadiabatic path integral [45], and the hierarchical equation of motion [46–48]. It turns out that the variational approach is capable of describing the non-Markovian dynamics of open quantum systems such as the spin-boson model and its variants in the strong system-reservoir coupling regime. An advantage of the variational approach over the master equation is that it retains both the reduced dynamics and the field dynamics. It is, therefore, feasible to calculate emission spectrum by passing the two-time correlation function and quantum regression theory [47]. Nevertheless, the performance of the variational approach should be further explored for the case of two qubits with a separation.

In this paper, we employ the time-dependent variational approach and analytical methods to study the emission spectra of two distant qubits strongly coupled to a one-dimensional waveguide beyond the weak-coupling regime and without using the RWA and the Markovian approximation. The variational method combines the Dirac-Frenkel time-dependent variational principle [49] with the multiple Davydov D_1 (multi-D_1) ansatz [44], which is found to be able to provide accurate results in certain strong-coupling regimes. We also attempt to calculate emission spectra with two analytical

*yiyingyan@zust.edu.cn

methods. One is based on the resolvent-operator formalism [50] and a transformed RWA (TRWA) Hamiltonian constructed from a unitary transformation that resembles the polaron transformation [28,51]. The other is the standard perturbation (SP) based on the resolvent-operator formalism and the original Hamiltonian. Comparisons between the variational results and the analytical results confirm the validity of the TRWA treatment while the SP treatment completely breaks down. By using the variational approach and the TRWA method, we illustrate that the emission spectrum is generally asymmetric and has a variety of line shapes, which can be single-peaked, vacuum-Rabi-splitting-like doublet, and complicated multipeaked depending on the distance and initial states. Under certain conditions, ultranarrow emission lines can be observed in the spectrum, indicating the subradiance. The present study reveals the emission spectral features of the two distant qubits in a strong light-matter coupling regime.

The rest of the paper is organized as follows. In Sec. II, we introduce the Hamiltonian and present both the numerical and analytical treatments for the emission spectrum. In Sec. III, we present the numerical results of the emission spectra and discuss the spectral features. In Sec. IV, the conclusions are drawn. Some technique details are presented in the Appendices.

II. MODEL AND METHODOLOGIES

We consider that two distant qubits are strongly coupled to a one-dimensional waveguide (reservoir), which is described by the Hamiltonian ($\hbar = 1$)

$$
H = \frac{\omega_0}{2} \sum_{j=1}^{2} \sigma_j^z + \sum_k \omega_k b_k^\dagger b_k
$$
$$
+ \sum_{j=1}^{2} \frac{\sigma_j^x}{2} \sum_k \lambda_k (b_k e^{-ikx_j} + b_k^\dagger e^{ikx_j}), \quad (1)
$$

where ω_0 is the transition frequency of the qubit, $\sigma_j^\mu (\mu = x, y, z)$ denotes the Pauli matrix for the jth qubit, x_j is the coordinate of the jth qubit, b_k ($b_k^\dagger$) is the annihilation (creation) operator of the kth bosonic mode with frequency ω_k of the reservoir, and λ_k is the coupling strength between the kth mode and the qubit. In this work, we assume $\lambda_k = \lambda_{-k}$ and a linear dispersion relation $\omega_k = v_g |k|$, where v_g is the propagating velocity of the photon in the waveguide. The wave numbers $k < 0$ and $k > 0$ are referred to as the left- and right-propagating field modes in the waveguide, respectively.

The dissipation of the waveguide is assumed to be characterized by the Ohmic spectral density function [38,52,53]:

$$
J(\omega) = \sum_k \lambda_k^2 \delta(\omega_k - \omega) = 2\alpha\omega\Theta(\omega_c - \omega), \quad (2)
$$

where α is a dimensionless coupling constant, $\Theta(\cdot)$ is the Heaviside function, and ω_c is the cutoff frequency. In the following, we use numerical and analytical methods to study the spontaneous emission of the two-qubit system.

A. Dirac-Frenkel time-dependent variational principle and multi-D_1 ansatz

In this section, we use the numerical approach that combines the Dirac-Frenkel time-dependent variational principle with the multi-D_1 ansatz to study the spontaneous emission. This approach is feasible to solve the time-dependent Schrödinger equation $i\frac{d}{dt}|\tilde{\psi}(t)\rangle = \tilde{H}(t)|\tilde{\psi}(t)\rangle$ in the interaction picture governed by the bath Hamiltonian $H_R = \sum_k \omega_k b_k^\dagger b_k$, where

$$
\tilde{H}(t) = \frac{\omega_0}{2} \sum_{j=1}^{2} \sigma_j^z + \sum_{j=1}^{2} \frac{\sigma_j^x}{2} \sum_k \lambda_k (b_k e^{-ikx_j - i\omega_k t} + \text{H.c.}).
$$
$$(3)$$

The Dirac-Frenkel time-dependent variational principle states that the optimal solution to the time-dependent Schrödinger equation can be found via [49]

$$
\langle \delta\tilde{\psi}(t) | i\partial_t - \tilde{H}(t) | \tilde{\psi}(t) \rangle = 0, \quad (4)
$$

where $|\tilde{\psi}(t)\rangle$ denotes a trial state and $\langle \delta\tilde{\psi}(t)|$ is the variation of the adjoint state of the trial state. Since the model under study in this work is a variant of the spin-boson model, we use the multi-D_1 ansatz, which has been found to be powerful in the spin-boson problem and takes the form [44]

$$
|D_1^M(t)\rangle = \sum_{j=1}^{4} \sum_{n=1}^{M} A_{nj} |\phi_j\rangle |f_{nj}\rangle, \quad (5)
$$

where M is the multiplicity, $|\phi_j\rangle \in \{|+\rangle|+\rangle, |+\rangle|-\rangle, |-\rangle|+\rangle, |-\rangle|-\rangle\}$ are the bases for the two-qubit system, and $|\pm\rangle$ are the eigenstates of the x-component Pauli matrix: $\sigma^x|\pm\rangle = \pm|\pm\rangle$. $|f_{nj}\rangle$ is the multimode coherent state used for the bosonic modes,

$$
|f_{nj}\rangle = \exp\left[\sum_k (f_{njk} b_k^\dagger - \text{H.c.}) \right] |0\rangle, \quad (6)
$$

where $|0\rangle$ is the multimode vacuum state of the reservoir. Supposing that the truncation numbers of the left- and right-propagating modes in the multi-D_1 ansatz are identical and given by N_b, we have introduced totally $4M(2N_b + 1)$ time-dependent variational parameters: A_{nj} and f_{njk}. The former represents the probability amplitude while the latter represents the displacement of the kth mode. One readily derives the equations of motion for these variational parameters by substituting the ansatz into Eq. (4), which yields

$$
i\langle\phi_j|\langle f_{mj}|\dot{D}_1^M(t)\rangle = \langle\phi_j|\langle f_{mj}|\tilde{H}(t)|D_1^M(t)\rangle, \quad (7)
$$

$$
i \sum_{j=1}^{4} A_{mj}^* \langle\phi_j|\langle f_{mj}|b_q|\dot{D}_1^M(t)\rangle
$$

$$
= \sum_{j=1}^{4} A_{mj}^* \langle\phi_j|\langle f_{mj}|b_q\tilde{H}(t)|D_1^M(t)\rangle. \quad (8)
$$

This is a set of nonlinear differential equations, which can be solved by using the Runge-Kutta method. We present the explicit form of the equations of motion and state the numerical implementation of the variational method in Appendix A.

To perform the numerical simulation, we use a finite truncated number of bath modes, $2N_b$, which can be derived from

a linear discretization of the spectral density. We divide the frequency domain $[0, \omega_c]$ into N_b equal intervals $[x_{n-1}, x_n]$, with $x_n = n\omega_c/N_b(n = 0, 1, 2, \ldots, N_b)$. The coupling constants and frequencies for the right-propagating modes $(k > 0)$ are determined by

$$\lambda_{k_n}^2 = \frac{1}{2} \int_{x_{n-1}}^{x_n} J(\omega)d\omega, \tag{9}$$

$$\omega_{k_n} = \frac{1}{2}\lambda_{k_n}^{-2} \int_{x_{n-1}}^{x_n} \omega J(\omega)d\omega, \tag{10}$$

where we have assumed that the left- and right-propagating modes contribute equally to the spectral density function and $1/2$ is used to cancel out the contribution from the left-propagating modes. The frequencies and coupling constants of the left-propagating modes can be obtained from the relations $\omega_k = \omega_{-k}$ and $\lambda_k = \lambda_{-k}$. The wave number is then specified via the relation $k_n = \pm\omega_{k_n}/v_g$. Throughout this work, we use $N_b = 300$ in the simulation, which is sufficient to yield convergent results when the final evolution time $t \leqslant 300\omega_0^{-1}$, $M < 10$, and $\alpha \leqslant 0.1$.

We are interested in the spontaneous emission process of the two-qubit system; thus, the initial state of the whole system is chosen as $|\psi(0)\rangle_S \otimes |0\rangle$, where $|\psi(0)\rangle_S$ is an initial state of the two-qubit system and the reservoir is initially in the vacuum state. In this work, we mainly consider three kinds of initial states of the two-qubit system: $\Psi_0 = |eg\rangle$ and $\Psi_\pm = (|eg\rangle \pm |ge\rangle)/\sqrt{2}$. Ψ_0 is a factorized state where the first qubit is in the excited state $|e\rangle$ and the second qubit is in the ground state $|g\rangle$. $\Psi_\pm$ are the symmetric and antisymmetric correlated (entangled) states, respectively.

On numerically solving the equations of motion, we can obtain both reduced dynamics of the qubits and the field dynamics. The excited-state population of the jth qubit can be calculated as

$$P_j^e(t) = \langle D_1^M(t)|\sigma_j^+\sigma_j^-|D_1^M(t)\rangle \quad (j = 1, 2), \tag{11}$$

where

$$\sigma_j^\pm = \left(\sigma_j^x \pm i\sigma_j^y\right)/2. \tag{12}$$

For the field, we are interested in the emission spectrum, which is defined as the number of photons with the frequency ω_k emitted into the reservoir at time t. The spontaneous emission spectrum is thus given by

$$N(\omega_k, t) = N(k, t) + N(-k, t), \tag{13}$$

where

$$N(k, t) = \langle D_1^M(t)|b_k^\dagger b_k|D_1^M(t)\rangle$$
$$= \sum_{j=1}^{4} \sum_{m,n=1}^{M} A_{mj}^* f_{mjk}^* \langle f_{mj}|f_{nj}\rangle f_{njk}A_{nj}, \tag{14}$$

is the photon number at the kth mode at the given time t. $\langle f_{mj}|f_{nl}\rangle$ is the overlap between the coherent states and is given by

$$\langle f_{mj}|f_{nl}\rangle = \exp\left[\sum_k \left(f_{mjk}^* f_{nlk} - \frac{|f_{mjk}|^2 + |f_{nlk}|^2}{2}\right)\right]. \tag{15}$$

The emission spectrum defined by $N(\omega_k, t)$ is generally time dependent. Nevertheless, the steady-state spectrum can be obtained in the long-time limit, i.e.,

$$N(\omega_k) = \lim_{t \to \infty} [N(k, t) + N(-k, t)]. \tag{16}$$

In simulation, we propagate the equations of motion for the variational parameters to a finial time of $t = 300\omega_0^{-1}$, which is sufficient to obtain steady-state spectra in most cases. The obtained spectra are referred to as the multi-D_1 results.

To measure the accuracy of the variational results, we calculate the scaled squared norm of the deviation vector [54],

$$\sigma^2(t) = \left|[i\partial_t - \tilde{H}(t)]|D_1^M(t)\rangle\right|^2/\omega_0^2$$
$$= \omega_0^{-2}\left[\langle D_1^M(t)|\tilde{H}^2(t)|D_1^M(t)\rangle - \langle \dot{D}_1^M(t)|\dot{D}_1^M(t)\rangle\right]. \tag{17}$$

The detailed calculation and behaviors of $\sigma^2(t)$ with the variation of t for the two-qubit spin-boson model are presented in the Appendix A. We find that the upper bound of the magnitude of $\sigma^2(t)$ in the interval $[0, 300\omega_0^{-1}]$ is of order 10^{-3} or 10^{-2} when $\alpha \leqslant 0.1$. This is sufficient to guarantee the accuracy of the variational results according to the previous work [47]. When $\alpha > 0.1$, it turns out that the variational method is accurate in short-time dynamics but becomes less reliable in long-time dynamics because of the increase in the error.

B. Analytical theory for spontaneous emission spectrum

In this section, we use two approximate approaches to analytically calculate the emission spectra with the resolvent-operator formalism [50]. In the first approach, we derive an effective Hamiltonian in a transformed frame and then combine it with the resolvent-operator formalism to evaluate the transition amplitude associated with the spontaneous emission process, which can be used to calculate the photon number at the kth mode in the long-time limit, $N(k)$. The steady spectrum is then obtained via Eq. (16). This treatment is referred to as the TRWA method. The second approach is similar to the first one but we use the original Hamiltonian, which is referred to as the SP.

To go beyond the weak-coupling regime, we apply a polaronlike unitary transformation to Eq. (1) [28,51],

$$H' = e^S H e^{-S}, \tag{18}$$

with the generator given by

$$S = \sum_{j=1}^{2} \sigma_j^x \sum_k \frac{\lambda_k}{2\omega_k}\xi_k(b_k^\dagger e^{ikx_j} - b_k e^{-ikx_j}), \tag{19}$$

where ξ_k are determined by requiring the first-order qubit-reservoir coupling to take the rotating-wave form in the transformed frame. Neglecting the higher-order qubit-reservoir coupling terms, we construct an effective Hamiltonian from the transformed Hamiltonian,

$$H' \approx H'_0 + H'_1, \tag{20}$$

$$H'_0 = \frac{1}{2}\eta\omega_0 \sum_{j=1}^{2} \sigma_j^z + \sum_k \omega_k b_k^\dagger b_k, \tag{21}$$

$$H'_1 = V_c\sigma_1^x\sigma_2^x + \sum_{j=1}^{2}\sum_k \tilde{\lambda}_k(\sigma_j^+ b_k e^{-ikx_j} + \sigma_j^- b_k^\dagger e^{ikx_j}), \tag{22}$$

where

$$\eta = \exp\left[-\frac{1}{2}\int_0^{\omega_c}\frac{J(x)dx}{(x+\eta\omega_0)^2}\right], \tag{23}$$

$$V_c = -\int_0^{\omega_c}\frac{J(x)(x+2\eta\omega_0)}{2(x+\eta\omega_0)}\cos\left(\frac{xd}{v_g}\right)dx, \tag{24}$$

$$d = x_1 - x_2, \tag{25}$$

$$\tilde{\lambda}_k = \frac{\lambda_k\eta\omega_0}{\eta\omega_0+\omega_k}. \tag{26}$$

This effective Hamiltonian is named as TRWA Hamiltonian. The detailed derivation of the TRWA Hamiltonian is presented in Appendix B.

Some remarks on the TRWA Hamiltonian are in order. First, it is worthwhile to note the important consequences of the qubit-reservoir coupling: the renormalization of the transition frequencies ($\eta\omega_0$) and a reservoir-induced dipole-dipole coupling ($V_c\sigma_1^x\sigma_2^x$). Physically, these effects arise from virtual photon processes and have been studied in Refs. [38,55] with similar approaches in the strong-coupling regime. Second, the qubit-reservoir interaction takes on the RWA-like form, which simplifies the mathematical treatment. Third, the total number of excitations of the TRWA Hamiltonian can be assumed to be conserved, which does not contradict the nonconservation of the total number of excitations in the laboratory frame [56]. This is because the excitation number operator $\hat{N} = \sum_{j=1}^2 \sigma_j^+\sigma_j^- + \sum_k b_k^\dagger b_k$ does not commute with the transformation generator S, which results in the excitation number in the transformed frame not being equal to that in the laboratory frame.

Combining the effective Hamiltonian with the resolvent-operator formalism, we calculate the photon number at the kth mode in the long-time limit for the three kinds of the two-qubit initial states when the reservoir is initially in the vacuum state. The detailed calculation is given in Appendix C. When the initial state of the two qubits is the factorized state Ψ_0, we find

$$N(k) = \tilde{\lambda}_k^2\left|\frac{\tilde{A}(\tilde{\omega}_k)+e^{-ikd}\tilde{B}(\tilde{\omega}_k)}{\tilde{A}^2(\tilde{\omega}_k)-\tilde{B}^2(\tilde{\omega}_k)}+\frac{1}{2\eta\omega_0}\right|^2, \tag{27}$$

where

$$\tilde{\omega}_k = \omega_k - \frac{V_c^2}{2\eta\omega_0}, \tag{28}$$

$$\tilde{A}(\omega) = \omega - \eta\omega_0 - \tilde{\Delta}(\omega,0) + i\tilde{\Gamma}(\omega,0), \tag{29}$$

$$\tilde{B}(\omega) = V_c + \tilde{\Delta}(\omega,d) - i\tilde{\Gamma}(\omega,d), \tag{30}$$

$$\tilde{\Delta}(\omega,d) = P\int_0^{\omega_c}\frac{J(x)\cos(xd/v_g)}{\omega-x}\left(\frac{\eta\omega_0}{x+\eta\omega_0}\right)^2 dx, \tag{31}$$

$$\tilde{\Gamma}(\omega,d) = \pi\left(\frac{\eta\omega_0}{\omega+\eta\omega_0}\right)^2 J(\omega)\cos\left(\frac{\omega d}{v_g}\right). \tag{32}$$

When the two-qubit initial state is $\Psi_\pm$, the photon number at the kth mode is found to be given by

$$N(k) = \tilde{\lambda}_k^2\left|\frac{1\pm e^{-ikd}}{\sqrt{2}}\right|^2\left|\frac{1}{\tilde{A}(\tilde{\omega}_k)\mp\tilde{B}(\tilde{\omega}_k)}+\frac{1}{2\eta\omega_0}\right|^2. \tag{33}$$

Interestingly, it seems that Eq. (33) is much simpler than Eq. (27), reflecting the fact that the spontaneous emission from the correlated states plays a more fundamental role than that from the factorized state [57,58]. In the following, the spectra obtained based on Eqs. (27) and (33) are referred to as the TRWA results.

To examine the improvement of the variational and TRWA method with respect to the SP, we further calculate the steady emission spectrum with the resolvent-operator formalism and the original Hamiltonian. The calculation details are presented in Appendix C. When the two-qubit initial state is Ψ_0, the photon number at the kth mode is given by

$$N(k) = \frac{\lambda_k^2}{4}\left|\frac{A(\omega_k')+e^{-ikd}B(\omega_k')}{A^2(\omega_k')-B^2(\omega_k')}\right|^2, \tag{34}$$

where

$$\omega_k' = \omega_k + 2\Delta(-\omega_0,0), \tag{35}$$

$$A(\omega) = \omega - \omega_0 - \Delta(\omega,0) - \Delta(\omega-2\omega_0,0)$$
$$+ i\Gamma(\omega,0) + i\Gamma(\omega-2\omega_0,0), \tag{36}$$

$$B(\omega) = \Delta(\omega,d) + \Delta(\omega-2\omega_0,d) - i\Gamma(\omega,d)$$
$$- i\Gamma(\omega-2\omega_0,d), \tag{37}$$

$$\Delta(\omega,d) = P\int_0^{\omega_c}\frac{J(x)\cos(xd/v_g)}{4(\omega-x)}dx, \tag{38}$$

$$\Gamma(\omega,d) = \frac{\pi}{4}J(\omega)\cos(\omega d/v_g). \tag{39}$$

When the two-qubit initial state is $\Psi_\pm$, the photon number at the kth mode is given by

$$N(k) = \frac{\lambda_k^2}{4}\left|\frac{\frac{1}{\sqrt{2}}(1\pm e^{-ikd})}{A(\omega_k')\mp B(\omega_k')}\right|^2. \tag{40}$$

Hereafter, the spectra calculated based on Eqs. (34) and (40) are referred to as the SP results. In the following we address the validity of the analytical results in comparison with the variational results.

III. NUMERICAL RESULTS AND DISCUSSIONS

In this section, we calculate the emission spectra by using the three methods: the variational method, the TRWA, and the SP. We make comparison between the multi-D_1 results and the analytical ones. This helps to clarify not only the emission spectral features but also the validity of the analytical treatments. Throughout this work, we set the cutoff frequency $\omega_c = 5\omega_0$ and define $L_0 \equiv v_g/\omega_0$ as a unit of distance. Physically, $2\pi L_0$ is equal to the wavelength of light of the angular frequency ω_0.

To begin with, let us address the consistency among the three approaches. Figure 1 shows the emission spectra calculated by the three methods for $\alpha = 0.05$ and for the three kinds of initial states and the three values of the two-qubit distance d. It is evident that the multi-D_1 results and the TRWA ones agree perfectly with each other, suggesting the validity of the latter. The SP results are found to be inconsistent with the multi-D_1 spectra. Particularly, for larger values of d, the SP
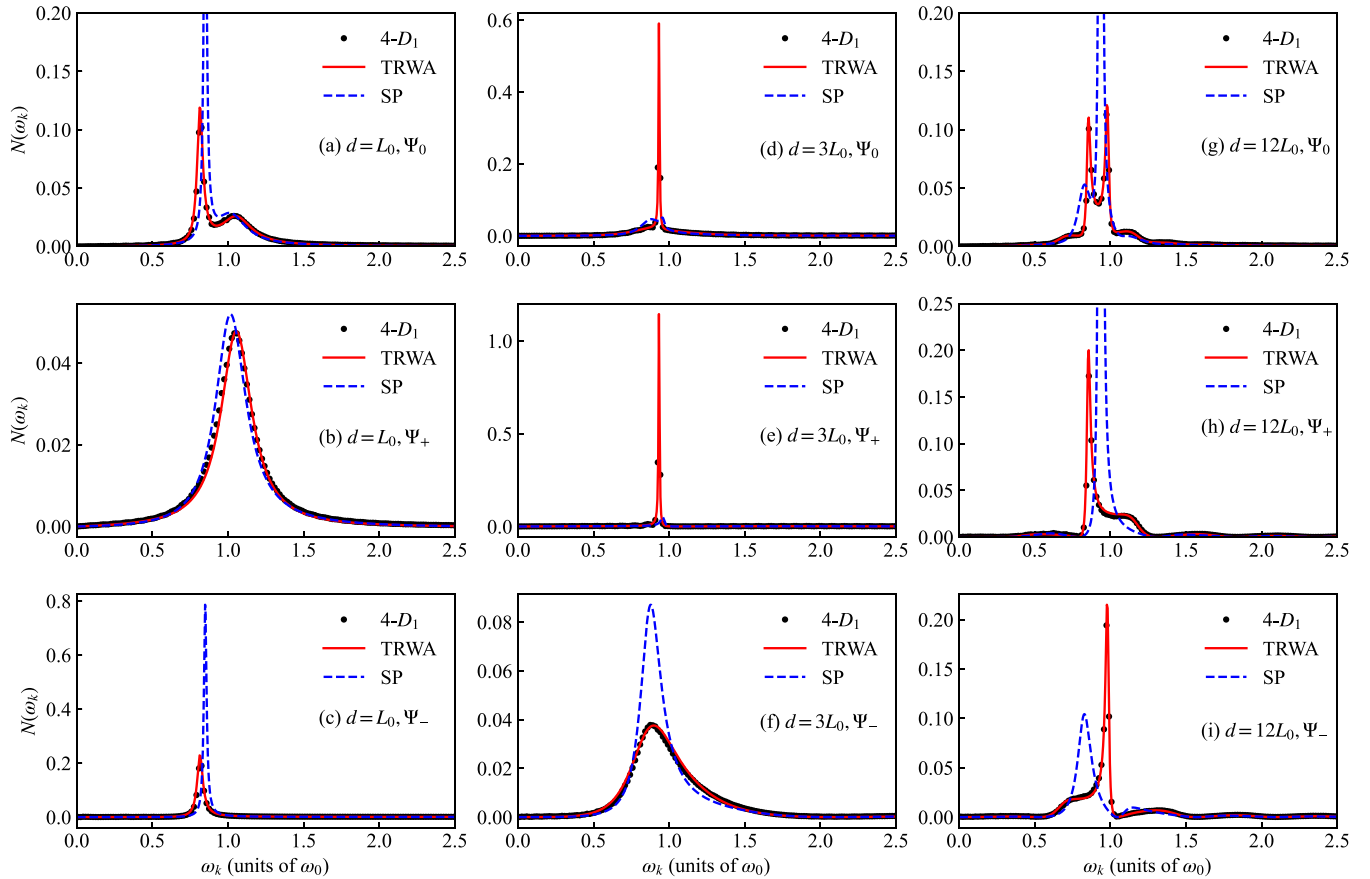
FIG. 1. Emission spectra calculated by the three methods for $\alpha = 0.05$, the three values of d, and the three kinds of initial states. "4-D_1" strands for the multi-D_1 result with the multiplicity $M = 4$.

results are strikingly different from the multi-D_1 results. The present results suggest that the variational method and the TRWA treatment are applicable to a strong-coupling regime where the SP treatment breaks down. Nevertheless, we should point out that the SP treatment and the TRWA treatment slightly differ from each other when $\alpha = 0.01$ and become indistinguishable from each other when $\alpha = 0.001$; that is, the two analytical approaches coincide in the weak-coupling regime.

To further examine the consistency between the variational method and the TRWA one, we employ the two methods to calculate the emission spectra for $\alpha = 0.1$ and for the three kinds of the initial states and the three values of d, which are shown in Fig. 2. We see that the TRWA results are satisfactorily accurate in comparison with the multi-D_1 results, confirming the validity of the TRWA method. It is worthwhile to note that in Figs. 2(g) and 2(h), there are more peaks in the multi-D_1 spectra than in the TRWA spectra. This difference can be attributed to the fact that the multi-D_1 spectra shown are not actually in the steady state; that is, we just propagate the equations of motion of the variational approach to the final time $t = 300\omega_0^{-1}$ and use $N(\omega_k, t)|_{t=300\omega_0^{-1}}$ to approximate the steady-state spectrum. This approximation may not be justified when a subradiant state with an utlraslow decay is encountered. We discuss such a phenomenon later. All in all, the present results show that the variational method and the TRWA treatment are applicable to the strong-coupling regime

when $\alpha \lesssim 0.1$. This is a significant improvement over the SP treatment which is justified when $\alpha \lesssim 0.01$. In addition, we should point out that the TRWA becomes less accurate when $\alpha > 0.1$ because the higher-order terms omitted in the TRWA should contribute, which has been explored in the dissipative Rabi and Jaynes-Cummings model [59].

Next, we focus on the multi-D_1 and TRWA results to analyze the emission spectral features of the two distant qubits. Figure 1(a) shows that, when $d = L_0$, the spectrum exhibits one narrow peak and one broad peak for the factorized initial state Ψ_0. In contrast, Figs. 1(b) and 1(c) show that the spectrum exhibits a single broad peak for the symmetric correlated initial state Ψ_+ and exhibits a single narrow peak for the antisymmetric correlated initial state Ψ_-, corresponding to the superradiant and subradiant states, respectively. Intuitively, it seems like that the formation of the doublet spectrum can be ascribed to the spontaneous emission from the correlated initial states. This situation is in analogy with the vacuum Rabi splitting which occurs in a qubit inside a cavity [60]. By using the analytical theory, we can figure out that the splitting between the two peaks is approximately given by $2|V_c + \tilde{\Delta}(\eta\omega_0, d)|$ when $d \sim L_0$, which depends on the reservoir-induced dipole-dipole coupling strength V_c and the Lamb shift $\tilde{\Delta}(\eta\omega_0, d)$.

Figures 1(d)–1(f) show that, when $d = 3L_0$, the spectrum exhibits a single peak for the three kinds of initial states. Moreover, the formation of the spectrum in Fig. 1(d) can be
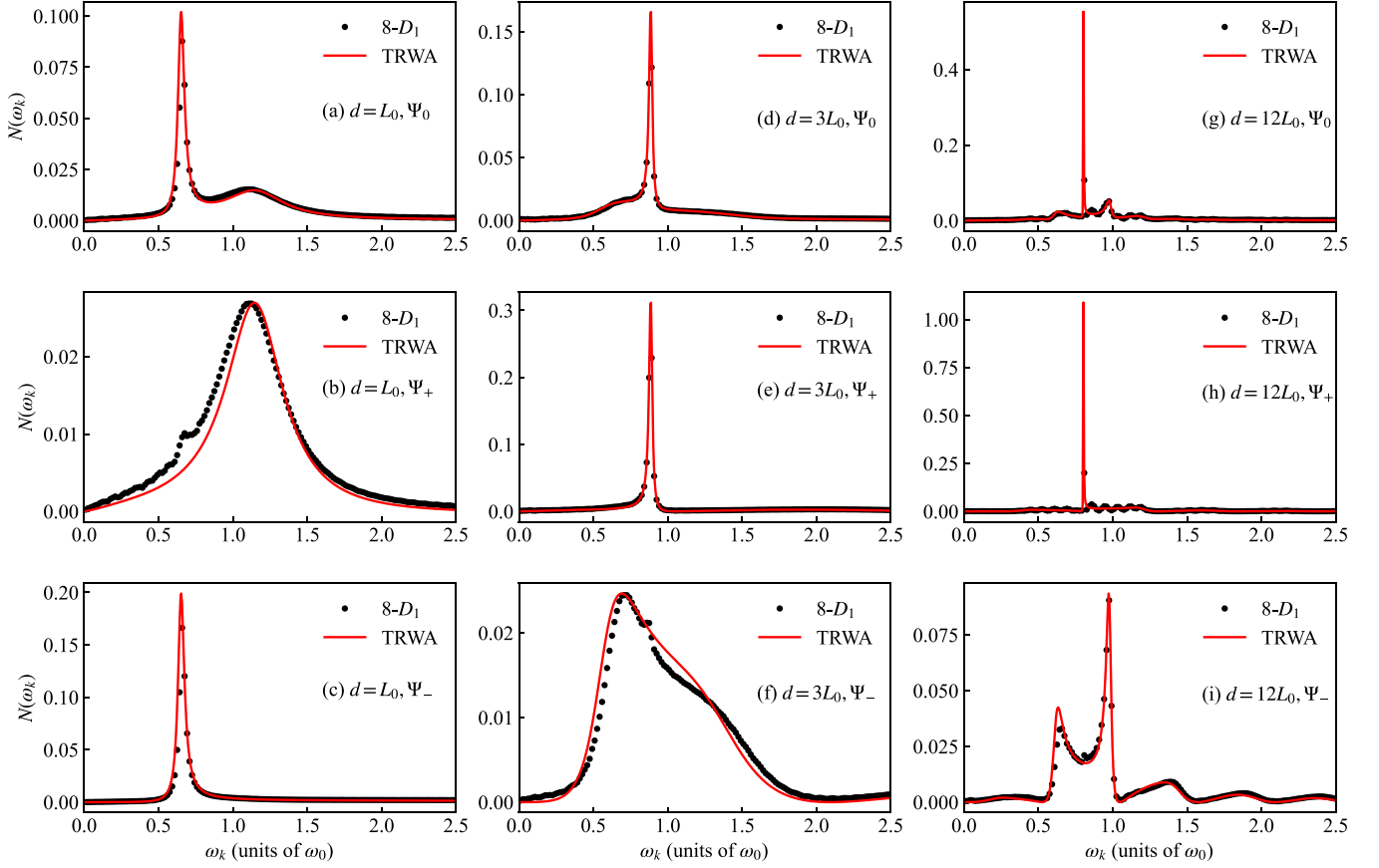
FIG. 2. Emission spectra calculated by the variational method and the TRWA method for $\alpha = 0.1$, the three values of d, and the three kinds of initial states.

understood as a result of the superposition of the spectrum in Figs. 1(e) and 1(f). It is worthwhile to note that the emission peak for the symmetric correlated initial state is very narrow, which indicates the occurrence of the subradiance. Figures 1(g)–1(i) show that, when the distance d further increases to $12L_0$, the spectrum is generally multipeaked for the three kinds of the initial states. The generation of the multipeaked spectrum is a result of the quantum interference of the radiating fields from the two distant qubits [37]. Besides, for large distances, the emission lines are, in general, sharply different from the typical Lorentzian lines, suggesting the

non-Markovian nature of the spontaneous emission process arising from the finite distance between the two qubits.

We now analyze in detail the change of the spectrum from the symmetric correlated initial state Ψ_+ due to the variation of the distance by using the TRWA analytical results (33) (which plays a fundamental role and a similar analysis can be carried out for the antisymmetric correlated initial state). To this end, we can simplify the spectrum by neglecting the constant term $1/(2\eta\omega_0)$, the contribution of which is relatively small. In doing so, we obtain the photon number at the kth mode,

$$N(k) \approx \frac{2\tilde{\lambda}_k^2 \cos^2\left(\frac{kd}{2}\right)}{[\tilde{\omega}_k - \eta\omega_0 - V_c - \tilde{\Delta}(\tilde{\omega}_k, 0) - \tilde{\Delta}(\tilde{\omega}_k, d)]^2 + \tilde{\Gamma}_+^2(\tilde{\omega}_k, d)}, \tag{41}$$

where

$$\tilde{\Gamma}_+(\omega, d) = 2\pi \left(\frac{\eta\omega_0}{\eta\omega_0 + \omega}\right)^2 J(\omega) \cos^2\left(\frac{\omega d}{2v_g}\right). \tag{42}$$

The emission spectrum is then given by $N(\omega_k) = N(k) + N(-k) = 2N(k)$ (which is a good approximate spectrum compared to the variational results). From the analytical result, we see that in the numerator and the denominator there are distance-dependent squared cosine functions, which reflects

the interference effect due to the field propagating between the two emitters. $\cos^2(kd/2)$ in the numerator simply leads to the multiple peaks for $d \gg L_0$. $\cos^2\left(\frac{\omega d}{2v_g}\right)$ in $\tilde{\Gamma}_+(\omega, d)$ may strongly alter the width of the emission line. To be specific, let us consider the values of $\tilde{\Gamma}_+(\omega, d)$ at $\omega = \eta\omega_0$ for different d, which are given by $\frac{\pi}{2}J(\eta\omega_0)\cos^2\left(\frac{\eta\omega_0 d}{2v_g}\right)$. Taking $\alpha = 0.05$, when $d = L_0$ and $d = 3L_0$, one finds that the squared cosine function $\cos^2\left(\frac{\eta\omega_0 d}{2v_g}\right)$ yields 0.7902 and 0.0204, respectively, suggesting a strong modification to the decay rate due to
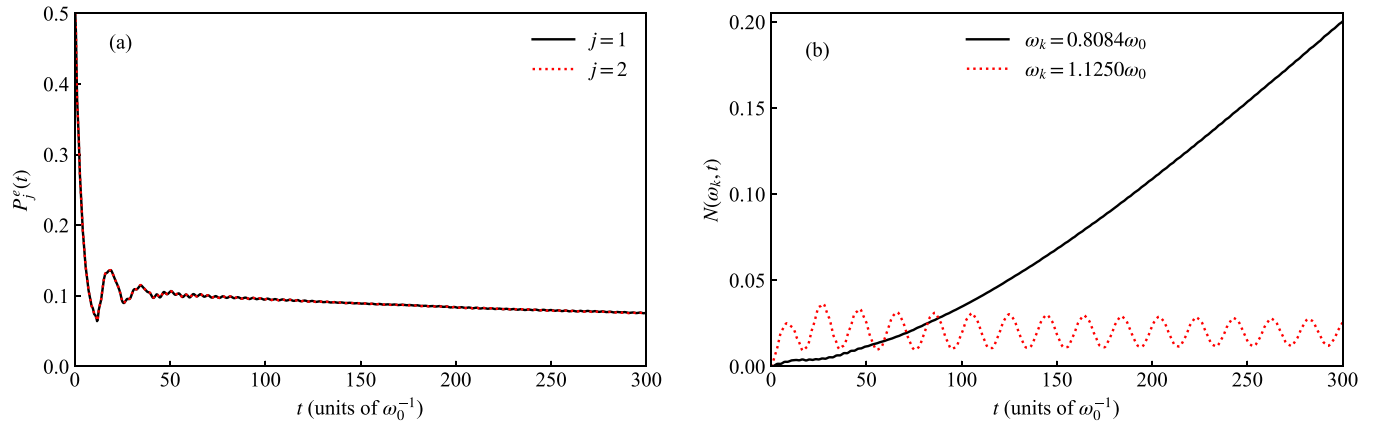
FIG. 3. (a) Excited-state population of the jth qubit $P_j^e(t)$ as a function of t obtained by the variational method. (b) Photon number $N(\omega_k, t)$ as a function of t obtained by the variational method for the two values of ω_k. The parameters are set as $\alpha = 0.1$ and $d = 12L_0$. The initial state is the symmetric correlated state Ψ_+.

the distance. This explains the change from a broad spectrum [Fig. 1(b)] to a narrow spectrum [Fig. 1(e)] due to the change of the distance. In addition, we note that as $d \to 0$, $\tilde{\Gamma}_+(\omega, d)$ becomes a slowly varying function of ω as long as α is relatively small and thus it is able to replace it with a constant decay rate [50], corresponding to a Markovian dynamical regime. However, if $d \gg L_0$, $\tilde{\Gamma}_+(\omega, d)$ is a fast-varying function of ω and is unable to be approximated by a constant decay rate. Thus the non-Markovian effects arise even in a weak-coupling regime [33].

From Fig. 2 we see that the spectral features in the case of $\alpha = 0.1$ are overall similar to those in the case of $\alpha = 0.05$. Besides, Fig. 2 further confirms that the spectra from the factorized initial state are composed of the emission lines arising from the two correlated states. Interestingly, we observe the ultranarrow emission lines in Figs. 2(g) and 2(h), signifying the subradiance. The present results suggest that the emission spectrum strongly depends on the distance of the two qubits, and the subradiance and superradiance may occur by tuning the distance. In addition, we find that the spectrum is generally asymmetric irrespective of the distance in the strong-coupling regime, in contrast with the RWA symmetric spectra in the weak-coupling regime [37].

We now discuss in detail the subradiance in Fig. 2(h), which results in the ultranarrow emission line in the TRWA spectrum as well as the inconsistency between the multi-D_1 and TRWA spectra in Figs. 2(g) and 2(h). To illustrate the subradiance, we employ the variational approach to calculate the dynamics of the excited-state population of the qubits as well as the dynamics of the photon number for $\alpha = 0.1$, $d = 12L_0$, and the symmetric correlated initial state. Figure 3(a) displays that the excited-state populations of the two qubits are identical and oscillate at short times, and as the time goes on such oscillation dies out and the populations ultraslowly decay with a vanishingly small beat behavior. The identical behaviors of the qubits can be ascribed to the symmetry of the Hamiltonian (1) and the initial state Ψ_+, which are invariant under the exchange of the qubits. The short-time oscillation is due to the dipole-dipole coupling, which is described by Eq. (C14) and physically related to the exchange of either real or virtual photons between the two qubits [52]. Clearly, the

qubits do not reach the steady state when $t = 300\omega_0^{-1}$. The steady-state populations can be calculated by [38]

$$\lim_{t \to \infty} P_j^e(t) = \langle \psi_G | \sigma_j^+ \sigma_j^- | \psi_G \rangle, \qquad (43)$$

where $|\psi_G\rangle$ is the ground state of the whole system and one can expect a nonvanishing steady value of the excited-state population due to the entangled light-matter ground state. Figure 3(b) displays that the photon number at $\omega_k = 0.8084\omega_0$ slowly increases with time while the photon number at $\omega_k = 1.1250\omega_0$ oscillates with an ultraslowly decaying amplitude, indicating that it takes a long time for the field to arrive at the steady state. The present finding suggests that even in the presence of a strongly dissipative reservoir, the spontaneous decay of the two qubits can be ultraslow due to the subradiance, which is in sharp contrast to the case of a single qubit strongly coupled to the reservoir [52].

IV. CONCLUSIONS

In summary, we have studied the emission spectrum of the two distant qubits strongly coupled to an Ohmic waveguide by using the variational approach and two analytical methods: TRWA and SP. The variational approach is based on the combination of the Dirac-Frenkel time-dependent variational principle and the multi-D_1 ansatz. The TRWA (SP) approach combines the resolvent-operator formalism and the TRWA (original) Hamiltonian, which allows us to derive the analytical spectrum function. The variational approach and the TRWA treatment are found to be consistent with each other and valid in certain strong-coupling regimes where the SP treatment breaks down. By using the variational and TRWA approaches we have illustrated that the emission spectrum of the two distant qubits is generally asymmetric and exhibits a single peak, double peaks, and multiple peaks depending on the distance and initial state of the two qubits. We have also elucidated that in spite of the strong coupling between the qubits and the reservoir, the occurrence of the subradiance leads to the fact that the two qubits and the radiation field ultraslowly reach their steady states. Our results provide insights

into the emission spectral features of the two distant qubits in the strong light-matter coupling regime.

The variational approach with the multi-D_1 ansatz allows us to go beyond the widely used RWA and the Born-Markovian approximation. This approach captures not only the reduced dynamics but also the field dynamics in a single simulation and can be further extended and applied to waveguide QED problems involving few multilevel emitters in strong light-matter coupling regimes.

APPENDIX A: EQUATIONS OF MOTION FOR THE VARIATIONAL PARAMETERS

To obtain the equations of motion for the variational parameters, we differentiate the multi-D_1 state with respect to t, which yields

$$|\dot{D}_1^M(t)\rangle = \sum_{j=1}^{4} \sum_{n=1}^{M} \left(a_{nj} + A_{nj} \sum_k \dot{f}_{njk} b_k^\dagger \right) |\phi_j\rangle |f_{nj}\rangle, \tag{A1}$$

where

$$a_{nj} = \dot{A}_{nj} - \frac{1}{2} A_{nj} \sum_k (\dot{f}_{njk} f_{njk}^* + f_{njk} \dot{f}_{njk}^*). \tag{A2}$$

By using the explicit form of the multi-D_1 state and its time derivative, it is straightforward to write the equations of motion (7) and (8) in terms of the variational parameters as follows:

$$0 = i \sum_{n=1}^{M} \left(a_{nj} + A_{nj} \sum_k f_{mjk}^* \dot{f}_{njk} \right) \langle f_{mj}|f_{nj}\rangle - \sum_{l=1}^{4} \sum_{n=1}^{M} \langle \phi_j|H_S|\phi_l\rangle A_{nl} \langle f_{mj}|f_{nl}\rangle$$

$$- \sum_{n=1}^{M} A_{nj} \sum_{h=1}^{2} \langle \phi_j|\sigma_h^x|\phi_j\rangle \sum_k \frac{\lambda_k}{2} (f_{mjk}^* e^{ikx_h + i\omega_k t} + f_{njk} e^{-ikx_h - i\omega_k t}) \langle f_{mj}|f_{nj}\rangle, \tag{A3}$$

$$0 = i \sum_{n=1}^{M} \left(\sum_{j=1}^{4} A_{mj}^* a_{nj} f_{njq} + \sum_{j=1}^{4} A_{mj}^* A_{nj} \sum_k (\delta_{k,q} + f_{mjk}^* f_{njq}) \dot{f}_{njk} \right) \langle f_{mj}|f_{nj}\rangle$$

$$- \sum_{j,l=1}^{4} \sum_{n=1}^{M} A_{mj}^* A_{nl} \langle \phi_j|H_S|\phi_l\rangle \langle f_{mj}|f_{nl}\rangle - \sum_{j=1}^{4} \sum_{n=1}^{M} A_{mj}^* A_{nj} \sum_{h=1}^{2} \langle \phi_j|\sigma_h^x|\phi_j\rangle$$

$$\times \sum_k \frac{\lambda_k}{2} [f_{njk} f_{njq} e^{-ikx_h - i\omega_k t} + (\delta_{k,q} + f_{mjk}^* f_{njq}) e^{ikx_h + i\omega_k t}] \langle f_{mj}|f_{nj}\rangle. \tag{A4}$$

These differential equations can be integrated by the following steps. First, we rewrite the above equations in the matrix form $i\mathcal{M}\vec{y} = \vec{\mathcal{I}}$, where $\mathcal{M}$ is the coefficient matrix, $\vec{y}$ is a vector consisting of a_{nj} and $\dot{f}_{njk}$, and $\vec{\mathcal{I}}$ is the inhomogeneous term. Second, the matrix equation is solved to yield the values of a_{nj} and $\dot{f}_{njk}$. $\dot{A}_{nj}$ is obtained via Eq. (A2). Third, the values of the derivatives are used to update the variational parameters based on the fourth-order Runge-Kutta algorithm.

The scaled squared norm of the deviation vector depends on the squared norm of $|\dot{D}_1^M(t)\rangle$ and the mean value of $\tilde{H}^2(t)$ over the multi-D_1 state, which can be formally calculated as follows:

$$\langle \dot{D}_1^M(t)|\dot{D}_1^M(t)\rangle = \sum_{j=1}^{4} \sum_{n,l=1}^{M} \left[a_{mj}^* a_{nj} + a_{mj}^* A_{nj} \sum_k \dot{f}_{njk} f_{mjk}^* + A_{mj}^* a_{nj} \sum_k \dot{f}_{mjk}^* f_{njk} + A_{mj}^* A_{nj} \sum_{k,q} (\delta_{k,q} + f_{mjk}^* f_{njq}) \dot{f}_{mjq}^* \dot{f}_{njk} \right]$$

$$\times \langle f_{mj}|f_{nj}\rangle, \tag{A5}$$

$$\langle \tilde{H}^2(t)\rangle = \langle D_1^M(t)|\tilde{H}^2(t)|D_1^M(t)\rangle$$

$$= \sum_{j,l=1}^{4} \sum_{n,m=1}^{M} A_{mj}^* A_{nl} \langle \phi_j|H_S^2|\phi_l\rangle \langle f_{mj}|f_{nl}\rangle + \sum_{j,l=1}^{4} \sum_{n,m=1}^{M} \sum_{h=1}^{2} A_{mj}^* \langle \phi_j|\{H_S, \sigma_h^x\}|\phi_l\rangle A_{nl} \sum_k \frac{\lambda_k}{2} (f_{mjk}^* e^{ikx_h + i\omega_k t} + f_{nlk} e^{-ikx_h - i\omega_k t})$$

$$\times \langle f_{mj}|f_{nl}\rangle + \sum_{j=1}^{4} \sum_{n,m=1}^{M} \sum_{h=1}^{2} A_{mj}^* A_{nj} \left\{ \left[\sum_k \frac{\lambda_k}{2} (f_{mjk}^* e^{ikx_h + i\omega_k t} + f_{njk} e^{-ikx_h - i\omega_k t}) \right]^2 + \sum_k \frac{\lambda_k^2}{4} \right\} \langle f_{mj}|f_{nj}\rangle$$

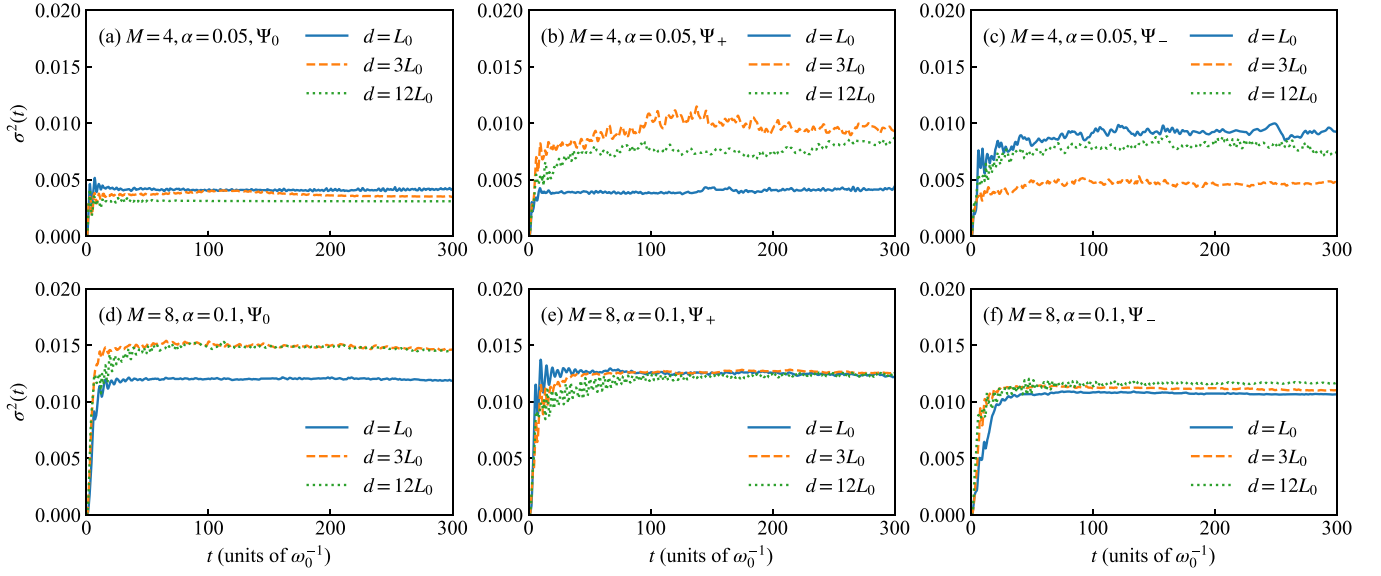FIG. 4. Scaled squared norm $\sigma^2(t)$ of the deviation vector as a function of time t for the two values of α, the three values of d, and the three kinds of initial states.

$$
+ 2 \sum_{j=1}^{4} \sum_{n,m=1}^{M} A_{mj}^* A_{nj} \langle \phi_j | \sigma_1^x \sigma_2^x | \phi_j \rangle \left[\sum_k \frac{\lambda_k}{2} (f_{mjk}^* e^{ikx_1 + i\omega_k t} + f_{njk} e^{-ikx_1 - i\omega_k t}) \right.
$$

$$
\left. \times \sum_q \frac{\lambda_q}{2} (f_{mjq}^* e^{iqx_2 + i\omega_q t} + f_{njq} e^{-iqx_2 - i\omega_q t}) + \sum_k \frac{\lambda_k^2}{4} \cos(kd) \right] \langle f_{mj} | f_{nj} \rangle. \tag{A6}
$$

In Fig. 4, we plot the behaviors of $\sigma^2(t)$ versus time for the two values of α, the three values of d, and the three kinds of the initial states. It turns out that the magnitude of $\sigma^2(t)$ takes on relatively small values, the order of which is 10^{-2} or smaller. This guarantees the reliability of the variational results [47].

APPENDIX B: DERIVATION OF THE EFFECTIVE HAMILTONIAN

The Hamiltonian in the transformed frame can be readily derived as follows:

$$
H' = e^S H e^{-S}
$$

$$
= \frac{\omega_0}{2} \sum_{j=1}^{2} \left(\sigma_j^z \cosh X_j - i \sigma_j^y \sinh X_j \right)
$$

$$
+ \sum_k \omega_k b_k^\dagger b_k + \sum_k \frac{\lambda_k^2}{2\omega_k} \left(\xi_k^2 - 2\xi_k \right)
$$

$$
+ \sum_{j=1}^{2} \frac{\sigma_j^x}{2} \sum_k \lambda_k (1 - \xi_k) \left(b_k e^{-ikx_j} + b_k^\dagger e^{ikx_j} \right)
$$

$$
+ \sum_k \frac{\lambda_k^2}{2\omega_k} \left(\xi_k^2 - 2\xi_k \right) \cos(kd) \sigma_1^x \sigma_2^x, \tag{B1}
$$

where

$$
X_j = \sum_k \frac{\lambda_k}{\omega_k} \xi_k \left(b_k^\dagger e^{ikx_j} - b_k e^{-ikx_j} \right). \tag{B2}
$$

We divide the transformed Hamiltonian into three parts:

$$
H' = H_0' + H_1' + H_2', \tag{B3}
$$

$$
H_0' = \frac{1}{2} \eta \omega_0 \sum_{j=1}^{2} \sigma_j^z + \sum_k \omega_k b_k^\dagger b_k + \sum_k \frac{\lambda_k^2}{2\omega_k} \left(\xi_k^2 - 2\xi_k \right), \tag{B4}
$$

$$
H_1' = \sum_{j=1}^{2} \frac{\sigma_j^x}{2} \sum_k \lambda_k (1 - \xi_k) \left(b_k e^{-ikx_j} + b_k^\dagger e^{ikx_j} \right)
$$

$$
- i \eta \omega_0 \sum_{j=1}^{2} \frac{\sigma_j^y}{2} \sum_k \frac{\lambda_k}{\omega_k} \xi_k \left(b_k^\dagger e^{ikx_j} - b_k e^{-ikx_j} \right)
$$

$$
+ V_c \sigma_1^x \sigma_2^x, \tag{B5}
$$

$$
H_2' = \frac{\omega_0}{2} \sum_{j=1}^{2} (\cosh X_j - \eta) \sigma_j^z - i \frac{\omega_0}{2} \sum_{j=1}^{2} (\sinh X_j - \eta X_j) \sigma_j^y, \tag{B6}
$$

where

$$
\eta = \langle 0 | \cosh X_j | 0 \rangle = \exp \left(-\frac{1}{2} \sum_k \frac{\lambda_k^2}{\omega_k^2} \xi_k^2 \right), \tag{B7}
$$

$$V_c = \sum_k \frac{\lambda_k^2}{2\omega_k}\left(\xi_k^2 - 2\xi_k\right)\cos(kd). \tag{B8}$$

To proceed, we reformulate the qubit-reservoir interaction in H_1' to be in the RWA form, which can be achieved by setting

$$\lambda_k(1 - \xi_k) = \eta\omega_0\frac{\lambda_k}{\omega_k}\xi_k. \tag{B9}$$

This equation results in $\xi_k = \frac{\omega_k}{\omega_k + \eta\omega_0}$ and $H_1' = V_c\sigma_1^x\sigma_2^x + \sum_{j=1}^{2}\sum_k \tilde{\lambda}_k(\sigma_j^+ b_k e^{-ikx_j} + \sigma_j^- b_k^\dagger e^{ikx_j})$. We should emphasis that the value of ξ_k can also be obtained by minimizing the ground-state energy of H_0'. Up till now we have not introduced any approximations.

To make the analytical calculation manageable, we use $H' \approx H_0' + H_1'$ as the effective Hamiltonian because H_2' comprises the second- and higher-order bosonic processes, the contribution of which is on the order of λ_k^4 and higher. This approximation is expected to be reasonable in a moderately strong coupling regime and is referred to as the TRWA.

APPENDIX C: ANALYTICAL CALCULATION OF SPONTANEOUS EMISSION SPECTRUM

Without loss of generality, we consider the initial state $|eg0\rangle \equiv |eg\rangle \otimes |0\rangle$. In the laboratory frame, the transition amplitude associated with the spontaneous emission process is given by

$$\langle gg1_k|U(t)|eg0\rangle, \tag{C1}$$

where $|gg1_k\rangle$ denotes the state that the two qubits are in the ground state and one photon occupies the kth mode of the reservoir, and $U(t) = \exp(-iHt)$ is the time-evolution operator of the whole system. The steady photon number at the kth mode is then calculated as

$$N(k) = \lim_{t \to \infty} |\langle gg1_k|U(t)|eg0\rangle|^2. \tag{C2}$$

We use the resolvent-operator formalism to calculate the transition amplitude. This formalism relates the time-evolution operator to the resolvent operator via the integral [50],

$$U(t) = \frac{1}{2\pi i}\int_{+\infty}^{-\infty} G(\omega + i0^+)e^{-i\omega t}d\omega \quad (t > 0), \tag{C3}$$

where

$$G(z) = \frac{1}{z - H} \tag{C4}$$

is the resolvent operator and z is a complex variable. In general, H is able to be divided into two parts: an exactly diagonalized H_0 and a perturbation V.

To calculate the matrix elements of the resolvent operator between some bases, e.g., the interested eigenstates of H_0, we introduce projectors $\mathcal{P}$ and $\mathcal{Q} = 1 - \mathcal{P}$, where $\mathcal{P}$ projects onto a subspace spanned by some interested eigenstates of H_0 and $\mathcal{Q}$ projects onto the complementary space. By using these projectors, we can derive the following equations from Eq. (C4):

$$\mathcal{P}(z - H)\mathcal{P}G(z)\mathcal{P} - \mathcal{P}V\mathcal{Q}G(z)\mathcal{P} = \mathcal{P}, \tag{C5}$$

$$\mathcal{Q}(z - H)\mathcal{Q}G(z)\mathcal{P} - \mathcal{Q}V\mathcal{P}G(z)\mathcal{P} = 0. \tag{C6}$$

The second equation can be solved to yield

$$\mathcal{Q}G(z)\mathcal{P} = \frac{1}{\mathcal{Q}(z - H)\mathcal{Q}}\mathcal{Q}V\mathcal{P}G(z)\mathcal{P}. \tag{C7}$$

Substituting this solution of $\mathcal{Q}G(z)\mathcal{P}$ into Eq. (C5), one readily obtains

$$\mathcal{P}G(z)\mathcal{P} = \frac{\mathcal{P}}{z - H_0 - \mathcal{P}R(z)\mathcal{P}}, \tag{C8}$$

where

$$R(z) = V + V\frac{\mathcal{Q}}{\mathcal{Q}(z - H)\mathcal{Q}}V$$

$$= V + V\frac{\mathcal{Q}}{z - H_0}V + \cdots \tag{C9}$$

is the level-shift operator. Using Eq. (C8), we can rewrite $\mathcal{Q}G(z)\mathcal{P}$ as

$$\mathcal{Q}G(z)\mathcal{P} = \frac{1}{\mathcal{Q}(z - H)\mathcal{Q}}\mathcal{Q}V\frac{\mathcal{P}}{z - H_0 - \mathcal{P}R(z)\mathcal{P}}. \tag{C10}$$

Similarly, one can derive the expression of $\mathcal{Q}G(z)\mathcal{Q}$ as follows:

$$\mathcal{Q}G(z)\mathcal{Q} = \frac{\mathcal{Q}}{z - \mathcal{Q}H\mathcal{Q}} + \frac{\mathcal{Q}}{z - \mathcal{Q}H\mathcal{Q}}V$$

$$\times \frac{\mathcal{P}}{z - H_0 - \mathcal{P}R(z)\mathcal{P}}V\frac{\mathcal{Q}}{z - \mathcal{Q}H\mathcal{Q}}. \tag{C11}$$

In the following, we show that the transition amplitudes associated with the spontaneous emission process can be derived from Eqs. (C8), (C10), and (C11).

1. Spontaneous emission spectrum with the unitary transformation

In this section, we calculate the transition amplitude with the effective Hamiltonian in the transformed frame. With the unitary transformation, we have

$$\langle gg1_k|U(t)|eg0\rangle = \langle gg1_k|e^{-S}e^S U(t)e^{-S}e^S|eg0\rangle$$

$$\approx \langle gg1_k|U'(t)|eg0\rangle + \sum_q \frac{\lambda_q}{2\omega_q}\xi_q e^{iqx_1}\langle gg1_k|U'(t)|gg1_q\rangle$$

$$- \frac{\lambda_k}{2\omega_k}\xi_k e^{ikx_1}\langle eg0|U'(t)|eg0\rangle - \frac{\lambda_k}{2\omega_k}\xi_k e^{ikx_2}\langle ge0|U'(t)|eg0\rangle, \tag{C12}$$

where we have used $e^S U(t) e^{-S} \approx \exp(-iH't) \equiv U'(t)$ and just retained the transition amplitudes associated with the single-excitation states. It is evident that in the transformed frame we need to evaluate four transition amplitudes with the transformed Hamiltonian H'.

Using $\mathcal{P} = |eg0\rangle\langle eg0| + |ge0\rangle\langle ge0|$ and setting H_0' and H_1' as the free and interaction Hamiltonians, respectively, we can derive the elements of the level-shift operator as follows:

$$\langle eg0|R(z)|eg0\rangle = \langle ge0|R(z)|ge0\rangle = \sum_q \frac{\tilde{\lambda}_q^2}{z + \eta\omega_0 - \omega_q}, \tag{C13}$$

$$\langle ge0|R(z)|eg0\rangle = \langle eg0|R(z)|ge0\rangle = V_c + \sum_q \frac{\tilde{\lambda}_q^2 \cos(qd)}{z + \eta\omega_0 - \omega_q}. \tag{C14}$$

It follows from Eq. (C8) that

$$\langle eg0|G(z)|eg0\rangle = \langle ge0|G(z)|ge0\rangle = \frac{z - \sum_q \frac{\tilde{\lambda}_q^2}{z+\eta\omega_0-\omega_q}}{\tilde{D}(z)}, \tag{C15}$$

$$\langle ge0|G(z)|eg0\rangle = \langle eg0|G(z)|ge0\rangle = \frac{V_c + \sum_q \frac{\tilde{\lambda}_q^2 \cos(qd)}{z+\eta\omega_0-\omega_q}}{\tilde{D}(z)}, \tag{C16}$$

where

$$\tilde{D}(z) = \left[z - \sum_q \frac{\tilde{\lambda}_q^2}{z + \eta\omega_0 - \omega_q} \right]^2 - \left[V_c + \sum_q \frac{\tilde{\lambda}_q^2 \cos(qd)}{z + \eta\omega_0 - \omega_q} \right]^2. \tag{C17}$$

Using Eq. (C10), we find

$$\langle gg1_k|G(z)|eg0\rangle = \langle gg1_k| \frac{\mathcal{Q}}{\mathcal{Q}(z - H')\mathcal{Q}} H_1' \mathcal{P} G(z) \mathcal{P} |eg0\rangle$$

$$= \langle gg1_k| \frac{\mathcal{Q}}{\mathcal{Q}(z - H')\mathcal{Q}} H_1' |eg0\rangle \langle eg0|G(z)|eg0\rangle + \langle gg1_k| \frac{\mathcal{Q}}{\mathcal{Q}(z - H')\mathcal{Q}} H_1' |ge0\rangle \langle ge0|G(z)|eg0\rangle$$

$$\approx \tilde{\lambda}_k e^{ikx_1} \langle gg1_k| \frac{\mathcal{Q}}{\mathcal{Q}(z - H')\mathcal{Q}} |gg1_k\rangle [\langle eg0|G(z)|eg0\rangle + e^{-ikd} \langle ge0|G(z)|eg0\rangle]$$

$$= \tilde{\lambda}_k e^{ikx_1} \frac{1}{z + \eta\omega_0 - \omega_k - \frac{V_c^2}{z-\eta\omega_0-\omega_k}} \left[\frac{z - \sum_q \frac{\tilde{\lambda}_q^2}{z+\eta\omega_0-\omega_q}}{\tilde{D}(z)} + e^{-ikd} \frac{V_c + \sum_q \frac{\tilde{\lambda}_q^2 \cos(qd)}{z+\eta\omega_0-\omega_q}}{\tilde{D}(z)} \right], \tag{C18}$$

where we have used

$$\langle gg1_k| \frac{\mathcal{Q}}{z - \mathcal{Q}H'\mathcal{Q}} |gg1_q\rangle \approx \frac{\delta_{k,q}}{z + \eta\omega_0 - \omega_k - \frac{V_c^2}{z-\eta\omega_0-\omega_k}}, \tag{C19}$$

which is derived from Eq. (C11).

To proceed, we should replace z with $\omega + i0^+$ in the matrix elements of the resolvent operator before integrating and use

$$\sum_q \frac{\tilde{\lambda}_q^2 \cos(qd)}{\omega - \omega_q + i0^+} = \tilde{\Delta}(\omega, d) - i\tilde{\Gamma}(\omega, d), \tag{C20}$$

where

$$\tilde{\Delta}(\omega, d) = P \sum_q \frac{\tilde{\lambda}_q^2 \cos(qd)}{\omega - \omega_q}, \tag{C21}$$

$$\tilde{\Gamma}(\omega, d) = \pi \sum_k \tilde{\lambda}_q^2 \cos(qd)\delta(\omega_q - \omega). \tag{C22}$$

In the long-time limit $t \to \infty$ and $d \neq 0$, the transition amplitudes given in Eq. (C12) can be evaluated as follows:

$$\langle eg0|U'(t)|eg0\rangle = \langle ge0|U'(t)|ge0\rangle = \frac{1}{2\pi i} \int_{\infty}^{-\infty} d\omega e^{-i\omega t} \frac{\tilde{A}(\omega + \eta\omega_0)}{\tilde{A}^2(\omega + \eta\omega_0) - \tilde{B}^2(\omega + \eta\omega_0)} = 0, \tag{C23}$$

$$\langle ge0|U'(t)|eg0\rangle = \langle eg0|U'(t)|ge0\rangle = \frac{1}{2\pi i}\int_{\infty}^{-\infty} d\omega e^{-i\omega t}\frac{\tilde{B}(\omega+\eta\omega_0)}{\tilde{A}^2(\omega+\eta\omega_0)-\tilde{B}^2(\omega+\eta\omega_0)} = 0, \tag{C24}$$

$$\langle gg1_k|U'(t)|gg1_p\rangle \approx \frac{1}{2\pi i}\int_{\infty}^{-\infty} d\omega e^{-i\omega t}\delta_{k,q}\frac{1}{\omega+i0^++\eta\omega_0-\omega_k-\frac{V_c^2}{\omega-\eta\omega_0-\omega_k}}$$

$$= \delta_{k,q}\exp\left[-i\left(\omega_k-\eta\omega_0-\frac{V_c^2}{2\eta\omega_0}\right)t\right], \tag{C25}$$

$$\langle gg1_k|U'(t)|eg0\rangle = \frac{1}{2\pi i}\int_{\infty}^{-\infty} d\omega e^{-i\omega t}\tilde{\lambda}_k e^{ikx_1}\frac{1}{\omega+i0^++\eta\omega_0-\omega_k-\frac{V_c^2}{\omega-\eta\omega_0-\omega_k}}\frac{\tilde{A}(\omega+\eta\omega_0)+e^{-ikd}\tilde{B}(\omega+\eta\omega_0)}{\tilde{A}^2(\omega+\eta\omega_0)-\tilde{B}^2(\omega+\eta\omega_0)}$$

$$= \tilde{\lambda}_k e^{ikx_1}\frac{\tilde{A}\left(\omega_k-\frac{V_c^2}{2\eta\omega_0}\right)+e^{-ikd}\tilde{B}\left(\omega_k-\frac{V_c^2}{2\eta\omega_0}\right)}{\tilde{A}^2\left(\omega_k-\frac{V_c^2}{2\eta\omega_0}\right)-\tilde{B}^2\left(\omega_k-\frac{V_c^2}{2\eta\omega_0}\right)}\exp\left[-i\left(\omega_k-\eta\omega_0-\frac{V_c^2}{2\eta\omega_0}\right)t\right], \tag{C26}$$

where we have used the fact that in the long-time limit the simple pole $\omega \approx \omega_k - \eta\omega_0 - \frac{V_c^2}{2\eta\omega_0}$ contributes to the steady state. $\tilde{A}(\omega)$ and $\tilde{B}(\omega)$ are defined in Eqs. (29) and (30) in the main text. Similarly, we also have

$$\langle gg1_k|U'(t)|ge0\rangle = \tilde{\lambda}_k e^{ikx_1}\frac{e^{-ikd}\tilde{A}\left(\omega_k-\frac{V_c^2}{2\eta\omega_0}\right)+\tilde{B}\left(\omega_k-\frac{V_c^2}{2\eta\omega_0}\right)}{\tilde{A}^2\left(\omega_k-\frac{V_c^2}{2\eta\omega_0}\right)-\tilde{B}^2\left(\omega_k-\frac{V_c^2}{2\eta\omega_0}\right)}\exp\left[-i\left(\omega_k-\eta\omega_0-\frac{V_c^2}{2\eta\omega_0}\right)t\right]. \tag{C27}$$

Using the above transition amplitudes, we can calculate the photon number at the kth mode in the long-time limit and thus derive the steady-state emission spectra.

2. Standard perturbation calculation

In this section, we calculate the spontaneous emission spectrum with the original Hamiltonian by setting $H_0 = \frac{\omega_0}{2}\sum_{j=1}^2\sigma_j^z + \sum_k\omega_k b_k^\dagger b_k$ and $V = \sum_{j=1}^2\frac{\sigma_j^x}{2}\sum_k\lambda_k(b_k e^{-ikx_j}+b_k^\dagger e^{ikx_j})$. Similarly, we use $\mathcal{P} = |eg0\rangle\langle eg0| + |ge0\rangle\langle ge0|$. The matrix elements of the level-shift operator can be computed up to the second order in λ_k as follows:

$$\langle eg0|R(z)|eg0\rangle = \langle ge0|R(z)|ge0\rangle$$

$$= \sum_q\left(\frac{\lambda_q^2/4}{z+\omega_0-\omega_q}+\frac{\lambda_q^2/4}{z-\omega_0-\omega_q}\right), \tag{C28}$$

$$\langle ge0|R(z)|eg0\rangle = \langle ge0|R(z)|eg0\rangle$$

$$= \sum_q\left(\frac{\lambda_q^2\cos(qd)/4}{z+\omega_0-\omega_q}+\frac{\lambda_q^2\cos(qd)/4}{z-\omega_0-\omega_q}\right). \tag{C29}$$

From Eq. (C8) one readily derives the following matrix elements:

$$\langle eg0|G(z)|eg0\rangle = \frac{z-\sum_q\left(\frac{\lambda_q^2/4}{z+\omega_0-\omega_q}+\frac{\lambda_q^2/4}{z-\omega_0-\omega_q}\right)}{D(z)}, \tag{C30}$$

$$\langle ge0|G(z)|eg0\rangle = \frac{\sum_q\left(\frac{\lambda_q^2\cos(qd)/4}{z+\omega_0-\omega_q}+\frac{\lambda_q^2\cos(qd)/4}{z-\omega_0-\omega_q}\right)}{D(z)}, \tag{C31}$$

where

$$D(z) = \left[z-\sum_q\left(\frac{\lambda_q^2/4}{z+\omega_0-\omega_q}+\frac{\lambda_q^2/4}{z-\omega_0-\omega_q}\right)\right]^2-\left[\sum_q\left(\frac{\lambda_q^2\cos(qd)/4}{z+\omega_0-\omega_q}+\frac{\lambda_q^2\cos(qd)/4}{z-\omega_0-\omega_q}\right)\right]^2. \tag{C32}$$

Using Eq. (C10), we have

$$\langle gg1_k|G(z)|eg0\rangle = \langle gg1_k|\frac{\mathcal{Q}}{\mathcal{Q}(z-H)\mathcal{Q}}V\mathcal{P}G(z)|eg0\rangle$$

$$= \langle gg1_k|\frac{\mathcal{Q}}{\mathcal{Q}(z-H)\mathcal{Q}}V|eg0\rangle\langle eg0|G(z)|eg0\rangle + \langle gg1_k|\frac{\mathcal{Q}}{\mathcal{Q}(z-H)\mathcal{Q}}V|ge0\rangle\langle ge0|G(z)|eg0\rangle$$

$$
\approx \frac{\lambda_k}{2} e^{ikx_1} \langle gg1_k| \frac{\mathcal{Q}}{\mathcal{Q}(z-H)\mathcal{Q}} |gg1_k\rangle \langle eg0|G(z)|eg0\rangle + \frac{\lambda_k}{2} e^{ikx_2} \langle gg1_k| \frac{\mathcal{Q}}{\mathcal{Q}(z-H)\mathcal{Q}} |gg1_k\rangle \langle ge0|G(z)|eg0\rangle
$$

$$
= \frac{\lambda_k}{2} e^{ikx_1} \langle gg1_k| \frac{\mathcal{Q}}{\mathcal{Q}(z-H)\mathcal{Q}} |gg1_k\rangle [\langle eg0|G(z)|eg0\rangle + e^{-ikd} \langle ge0|G(z)|eg0\rangle]
$$

$$
= \frac{\lambda_k}{2} e^{ikx_1} \frac{1}{z + \omega_0 - \omega_k - \frac{1}{2}\sum_q \frac{\lambda_q^2}{z-\omega_k-\omega_q}}
$$

$$
\times \frac{z - \sum_q \left(\frac{\lambda_q^2/4}{z+\omega_0-\omega_q} + \frac{\lambda_q^2/4}{z-\omega_0-\omega_q} \right) + e^{-ikd} \sum_q \left(\frac{\lambda_q^2 \cos(qd)/4}{z+\omega_0-\omega_q} + \frac{\lambda_q^2 \cos(qd)/4}{z-\omega_0-\omega_q} \right)}{D(z)}, \tag{C33}
$$

where we have used

$$
\langle gg1_k| \frac{\mathcal{Q}}{\mathcal{Q}(z-H)\mathcal{Q}} |gg1_k\rangle \approx \frac{1}{z + \omega_0 - \omega_k - \frac{1}{2}\sum_q \frac{\lambda_q^2}{z-\omega_k-\omega_q}}. \tag{C34}
$$

Similarly, we have

$$
\langle gg1_k|G(z)|ge0\rangle = \frac{\lambda_k}{2} e^{ikx_1} \frac{1}{z + \omega_0 - \omega_k - \frac{1}{2}\sum_q \frac{\lambda_q^2}{z-\omega_k-\omega_q}}
$$

$$
\times \frac{e^{-ikd}\left[z - \sum_q \left(\frac{\lambda_q^2/4}{z+\omega_0-\omega_q} + \frac{\lambda_q^2/4}{z-\omega_0-\omega_q} \right)\right] + \sum_q \left(\frac{\lambda_q^2 \cos(qd)/4}{z+\omega_0-\omega_q} + \frac{\lambda_q^2 \cos(qd)/4}{z-\omega_0-\omega_q} \right)}{D(z)}, \tag{C35}
$$

To perform the integral we replace z with $\omega + i0^+$ and use

$$
\sum_q \frac{\lambda_q^2 \cos(qd)/4}{\omega - \omega_q + i0^+} = \Delta(\omega, d) - i\Gamma(\omega, d), \tag{C36}
$$

where

$$
\Delta(\omega, d) = P \sum_q \frac{\lambda_q^2 \cos(qd)/4}{\omega - \omega_q}, \tag{C37}
$$

$$
\Gamma(\omega, d) = \frac{\pi}{4} \sum_q \lambda_q^2 \cos(qd)\delta(\omega - \omega_q). \tag{C38}
$$

In the long-time limit, we have

$$
\langle gg1_k|U(t)|eg0\rangle = \frac{1}{2\pi i} \int_{+\infty}^{-\infty} \langle gg1_k|G(\omega + i0^+)|eg0\rangle e^{-i\omega t} d\omega
$$

$$
= \frac{1}{2\pi i} \int_{+\infty}^{-\infty} \frac{\lambda_k}{2} e^{ikx_1} \frac{1}{\omega + i0^+ + \omega_0 - \omega_k - 2\Delta(\omega - \omega_k, 0)} \times \frac{A(\omega + \omega_0) + e^{-ikd}B(\omega + \omega_0)}{A^2(\omega + \omega_0) - B^2(\omega + \omega_0)} e^{-i\omega t} d\omega
$$

$$
\approx \frac{\lambda_k}{2} e^{ikx_1} \frac{A[\omega_k + 2\Delta(-\omega_0, 0)] + e^{-ikd}B[\omega_k + 2\Delta(-\omega_0, 0)]}{A^2[\omega_k + 2\Delta(-\omega_0, 0)] - B^2[\omega_k + 2\Delta(-\omega_0, 0)]} e^{-i[\omega_k - \omega_0 + 2\Delta(-\omega_0, 0)]t}, \tag{C39}
$$

$$
\langle gg1_k|U(t)|ge0\rangle = \frac{1}{2\pi i} \int_{+\infty}^{-\infty} \langle gg1_k|G(\omega + i0^+)|ge0\rangle e^{-i\omega t} d\omega
$$

$$
= \frac{1}{2\pi i} \int_{+\infty}^{-\infty} d\omega e^{-i\omega t} \frac{\lambda_k}{2} e^{ikx_1} \frac{1}{\omega + i0^+ + \omega_0 - \omega_k - 2\Delta(\omega - \omega_k, 0)} \times \frac{e^{-ikd}A(\omega + \omega_0) + B(\omega + \omega_0)}{A^2(\omega + \omega_0) - B^2(\omega + \omega_0)}
$$

$$
\approx \frac{\lambda_k}{2} e^{ikx_1} \frac{e^{-ikd}A[\omega_k + 2\Delta(-\omega_0, 0)] + B[\omega_k + 2\Delta(-\omega_0, 0)]}{A^2[\omega_k + 2\Delta(-\omega_0, 0)] - B^2[\omega_k + 2\Delta(-\omega_0, 0)]} e^{-i[\omega_k - \omega_0 + 2\Delta(-\omega_0, 0)]t}, \tag{C40}
$$

where $A(\omega)$ and $B(\omega)$ are defined in Eqs. (36) and (37) in the main text, respectively, and we have used the fact that the simple pole $\omega \approx \omega_k - \omega_0 + 2\Delta(-\omega_0, 0)$ determined from $\omega + \omega_0 - \omega_k - 2\Delta(\omega - \omega_k, 0) = 0$ contributes to the long-time behavior. Using the above results, it is straightforward to calculate the emission spectra for the three kinds of the initial states.

[1] P. Samutpraphoot, T. Đorđević, P. L. Ocola, H. Bernien, C. Senko, V. Vuletić, and M. D. Lukin, Phys. Rev. Lett. **124**, 063602 (2020).

[2] L. Ma, X. Lei, J. Cheng, Z. Yan, and X. Jia, Opt. Express **31**, 8257 (2023).

[3] J. Cho and H.-W. Lee, Phys. Rev. A **72**, 052309 (2005).

[4] S.-B. Zheng, Appl. Phys. Lett. **94**, 154101 (2009).

[5] R. Wiegner, J. von Zanthier, and G. S. Agarwal, Phys. Rev. A **84**, 023805 (2011).

[6] A. Lee, H. S. Han, F. K. Fatemi, S. L. Rolston, and K. Sinha, Phys. Rev. A **107**, 013701 (2023).

[7] M. T. Raiford, Phys. Rev. A **9**, 1257 (1974).

[8] C.-r. Fu and C-d. Gong, Phys. Rev. A **45**, 5095 (1992).

[9] K. Ujihara and H. T. Dung, Phys. Rev. A **66**, 053807 (2002).

[10] M. Macovei and C. H. Keitel, Phys. Rev. Lett. **91**, 123601 (2003).

[11] A. A. Makarov and V. S. Letokhov, J. Exp. Theor. Phys. **97**, 688 (2003).

[12] S. Zeeb, C. Noh, A. S. Parkins, and H. J. Carmichael, Phys. Rev. A **91**, 023829 (2015).

[13] R. Reimann, W. Alt, T. Kampschulte, T. Macha, L. Ratschbacher, N. Thau, S. Yoon, and D. Meschede, Phys. Rev. Lett. **114**, 023601 (2015).

[14] D. Bhatti, R. Schneider, S. Oppel, and J. von Zanthier, Phys. Rev. Lett. **120**, 113603 (2018).

[15] M.-O. Pleinert, J. von Zanthier, and G. S. Agarwal, Phys. Rev. A **97**, 023831 (2018).

[16] P.-O. Guimond, A. Grankin, D. V. Vasilyev, B. Vermersch, and P. Zoller, Phys. Rev. Lett. **122**, 093601 (2019).

[17] P. R. Berman, Phys. Rev. A **101**, 013830 (2020).

[18] Y. S. Greenberg and O. A. Chuikin, Eur. Phys. J. B **95**, 151 (2022).

[19] P. Solano, P. Barberis-Blostein, and K. Sinha, Phys. Rev. A **107**, 023723 (2023).

[20] S. Richter, S. Wolf, J. von Zanthier, and F. Schmidt-Kaler, Phys. Rev. Res. **5**, 013163 (2023).

[21] P. W. Milonǹi and P. L. Knight, Phys. Rev. A **11**, 1090 (1975).

[22] S. Rist, J. Eschner, M. Hennrich, and G. Morigi, Phys. Rev. A **78**, 013808 (2008).

[23] A. F. van Loo, A. Fedorov, K. Lalumière, B. C. Sanders, A. Blais, and A. Wallraff, Science **342**, 1494 (2013).

[24] G. Díaz-Camacho, D. Porras, and J. J. García-Ripoll, Phys. Rev. A **91**, 063828 (2015).

[25] P. Zhao, X. Tan, H. Yu, S.-L. Zhu, and Y. Yu, Phys. Rev. A **95**, 063848 (2017).

[26] Z. Ficek and R. Tanaś, Phys. Rep. **372**, 369 (2002).

[27] C. Lazarou and B. M. Garraway, Phys. Rev. A **77**, 023818 (2008).

[28] X.-F. Cao and H. Zheng, Eur. Phys. J. B **68**, 209 (2009).

[29] X.-Y. Lü, L.-G. Si, X.-Y. Hao, and X. Yang, Phys. Rev. A **79**, 052330 (2009).

[30] H. Nihira and C. R. Stroud, Phys. Rev. A **80**, 042329 (2009).

[31] K. Almutairi, R. Tanaś, and Z. Ficek, Phys. Rev. A **84**, 013831 (2011).

[32] Y. Wang, J. Ren, W. Zhang, L. He, and X. Zhang, Phys. Rev. Appl. **14**, 054007 (2020).

[33] K. Sinha, P. Meystre, E. A. Goldschmidt, F. K. Fatemi, S. L. Rolston, and P. Solano, Phys. Rev. Lett. **124**, 043603 (2020).

[34] A. F. Kockum, A. Miranowicz, S. D. Liberato, S. Savasta, and F. Nori, Nat. Rev. Phys. **1**, 19 (2019).

[35] P. Forn-Díaz, L. Lamata, E. Rico, J. Kono, and E. Solano, Rev. Mod. Phys. **91**, 025005 (2019).

[36] P. Y. Wen, K.-T. Lin, A. F. Kockum, B. Suri, H. Ian, J. C. Chen, S. Y. Mao, C. C. Chiu, P. Delsing, F. Nori, G.-D. Lin, and I.-C. Hoi, Phys. Rev. Lett. **123**, 233602 (2019).

[37] K. Sinha, A. González-Tudela, Y. Lu, and P. Solano, Phys. Rev. A **102**, 043718 (2020).

[38] C. A. González-Gutiérrez, J. Román-Roche, and D. Zueco, Phys. Rev. A **104**, 053701 (2021).

[39] Y. Zhao, J. Chem. Phys. **158**, 080901 (2023).

[40] M. Werther and F. Grossmann, Phys. Scr. **93**, 074001 (2018).

[41] L. Chen and Y. Zhao, J. Chem. Phys. **147**, 214102 (2017).

[42] M. Werther and F. Großmann, Phys. Rev. B **101**, 174315 (2020).

[43] P. P. Orth, D. Roosen, W. Hofstetter, and K. Le Hur, Phys. Rev. B **82**, 144423 (2010).

[44] T. Deng, Y. Yan, L. Chen, and Y. Zhao, J. Chem. Phys. **144**, 144102 (2016).

[45] Y. Fujihashi, L. Wang, and Y. Zhao, J. Chem. Phys. **147**, 234107 (2017).

[46] L. Wang, L. Chen, N. Zhou, and Y. Zhao, J. Chem. Phys. **144**, 024101 (2016).

[47] Y. Yan, L. Chen, J. Y. Luo, and Y. Zhao, Phys. Rev. A **102**, 023714 (2020).

[48] L. Chen, Y. Yan, M. F. Gelin, and Z. Lü, J. Chem. Phys. **158**, 104109 (2023).

[49] J. Frenkel, *Wave Mechanics* (Oxford University, Oxford, 1934).

[50] C. Cohen-Tannoudji, J. Dupont-Roc, and G. Grynberg, *Atom-Photon Interactions: Basic Processes and Applications* (Wiley-VCH, Weinheim, 2004).

[51] H. Zheng, Eur. Phys. J. B **38**, 559 (2004).

[52] G. Díaz-Camacho, A. Bermudez, and J. J. García-Ripoll, Phys. Rev. A **93**, 043843 (2016).

[53] T. Shi, Y. Chang, and J. J. García-Ripoll, Phys. Rev. Lett. **120**, 153602 (2018).

[54] R. Martinazzo and I. Burghardt, Phys. Rev. Lett. **124**, 150601 (2020).

[55] D. P. S. McCutcheon, A. Nazir, S. Bose, and A. J. Fisher, Phys. Rev. B **81**, 235321 (2010).

[56] S. D. Liberato, Nat. Commun. **8**, 1465 (2017).

[57] P. Facchi, M. S. Kim, S. Pascazio, F. V. Pepe, D. Pomarico, and T. Tufarelli, Phys. Rev. A **94**, 043839 (2016).

[58] P. Facchi, S. Pascazio, F. V. Pepe, and D. Pomarico, Phys. Rev. A **98**, 063823 (2018).

[59] C. Zhang, M. Yu, Y. Yan, L. Chen, Z. Lü, and Y. Zhao, J. Chem. Phys. **157**, 214116 (2022).

[60] L. S. Bishop, J. M. Chow, J. Koch, A. A. Houck, M. H. Devoret, E. Thuneberg, S. M. Girvin, and R. J. Schoelkopf, Nat. Phys. **5**, 105 (2009).